X-ray Diffraction Analysis of the Particulate Matter in Residual Oil Flyash

A. Manivannan and M. S. Seehra
Physics Department, West Virginia University,
PO Box: 6315, Morgantown, WV 226506-6315

KEYWORDS: Particulate Matter, Characterization, X-ray Diffraction

ABSTRACT

X-ray diffraction studies are reported on a series of PM samples produced by combustion of residual fuel oil. The residual oil flyash (ROFA) from four oils of varying sulfur content were aerodynamically separated into <2.5 micron and >2.5 micron fractions using a cyclone. The analysis of their x-ray diffraction measurements indicated sharp lines due to the presence of crystalline components superposed on two broad peaks due to amorphous carbon. The intensity of the crystalline components tends to be higher in the <2.5 micron fractions and in oils with the higher sulfur content. The sharp lines have been identified with various sulfites and sulfates of Zn, V, Ni, Pb, Fe, Cu and Ca.

INTRODUCTION

Particulate Matter (PM) is composed of a mixture of particles directly emitted into the air and the particles formed in air from the chemical transformation of gaseous pollutants (secondary particles). The earlier focus of the US Environmental Protection Agency (EPA) was on the particulate matter less than 10 microns in diameter (PM_{10}). In July 1997, EPA adopted a new rule that, for the first time, addressed particulate matter with diameter less than 2.5 microns (fine PM or $PM_{2.5}$) [1]. The implementation of this new rule requires the acquisition of important scientific information regarding the effects of $PM_{2.5}$ on public health and welfare. These adverse health effects include premature mortality, aggravation of respiratory and cardiovascular symptoms and illness, change in lung structure, and altered respiratory defense mechanisms [2-4]. Two controversial studies (the Harvard University six-city study and the American Cancer Society study) have linked the presence of fine particular matter to premature mortality [5]. Generally, fine particles are considered to be more hazardous than coarse particles. Therefore, the analysis have to be done at molecular levels. In order to understand the molecular speciation and its parameters such as valency, solubility, acidity, and composition, it is essential to identify and analyze the elements and compounds present accurately by employing several analytical tools. Huffman et al., have carried out X-ray absorption fine structure (XAFS) analysis to investigate several elements in ROFA samples [6].

In this work, we have employed x-ray diffraction for the identification and analysis of the compounds present in $PM_{2.5}$ samples. The technique of x-ray diffraction allows identification of any crystalline material, elements or compounds, present in a sample. In this work, x-ray diffraction was used to investigate the suite of residual oil flyash (ROFA) samples separated aerodynamically into fractions <2.5 ($PM_{2.5}$) and >2.5 microns ($PM_{2.5+}$) in diameter. The ROFA samples were generated by combustion of residual fuel oil at the EPA laboratory at the Research Triangle Park in experiments conducted by Miller et al [7]. A series of eight samples were analysed. All the PM samples measured possess sharp lines superposed on two broad peaks. We could identify the sharp lines due to various sulfates of Zn, V, Ni, Pb Fe, Cu and Ca. The two broad peaks are due to presence of amorphous carbon [8].

EXPERIMENTAL

The combustion experiments were carried out in a North American three-pass fire tube package boiler, which is a practical, commercially available heavy fuel oil combustion unit. A detailed description of this boiler is given elsewhere [7]. Samples were

separated aerodynamically by a cyclone into fractions that were nominally < and > 2.5 microns in diameter, hereafter referred to as $PM_{2.5}$ and $PM_{2.5+}$. The sampling system consists of a large dilution sampler capable of isokinetically sampling 0.28m^3/mmin (10ft^3/min) of flue gas using a Source Assessment Sampling System (SASS) cyclone. The SASS cyclone produces 50 and 95% collection efficiencies at approximately 1.8 and 2.5 micron diameter, respectively. The resulting PM is collected on large (65 cm) Teflon coated glass fiber filters, transferred to sampling jars, and made available for analysis.

Although burnout was fairly complete (>99.7%), the inorganic content of the oils was quite low (0.02-0.10 wt.% ash), and the dominant element of the ROFA is carbon. Loss on ignition (LOI) measurements indicate that the carbon content of the $PM_{2.5}$ ranged from 64 to 87 wt.% and that of the $PM_{2.5+}$ from 88 to 97%. S content of the PM samples was ~ 1 to several wt.%, while the V content ranged from 0.5 to 5.9 wt.% and the Ni content from 0.08 to 0.8 wt.%. As reported in the paper by Miller et al. [7], the metals are typically more concentrated in the $PM_{2.5}$ samples than they are in the $PM_{2.5+}$ samples by factors ~3 to 6.

These samples were investigated using a Wide Angle X-ray Diffractometer (WAXD). The WAXD used is a Rigaku diffractometer (Model D/MAX) using Cu Kα radiation with a wavelength λ of 1.542 Å. The other experimental conditions include ½° divergence and scatter slits, 0.15mm receiving slits, step scans with 0.04° steps and 30sec, counting time at each step, and intensity measured in counts. This relatively slow scan process enabled us to obtain the diffraction pattern with resolved sharp lines due to various compounds. The analysis of the X-ray patterns have been carried out using Jade software package produce by MDI (Materials Data Inc.) and the JCPDS data files.

RESULTS AND DISCUSSION

The X-ray diffraction patterns of the two ROFA samples (oil #5) are shown in Figures 1 (<2.5 microns) and 2 (>2.5 microns). Figure 1 shows well defined sharp lines superposed on two broad peaks at $2\theta \equiv 26°$ and 44°) due to amorphous carbon[8]. The inorganic components have been identified as $CaSO_4$; $Zn_4SO_4(OH)_6 \cdot 5H_2O$; $Zn(SO_3) \cdot 2.5H_2O$; $VOSO_4$; $NiSO_4 \cdot 6H_2O$; PbS_2O_3; $Fe_3(SO_4)_4 \cdot 14H_2O$; $ZnSO_4 \cdot xH_2O$; $Ca(SO_4)(H_2O)_2$; Cu_2SO_4. All these phases are identified and labeled as shown in the Figs. 1, 2 and 3. Figure 2 shows only $CaSO_4$ phase and the two broad peaks due to carbon [7]. In a similar fashion a total of eight samples were analyzed and the inorganic phases identified are summarized in Table 1. The samples are found to contain various sulfates and sulfites of Zn, V, Ni, Pb, Fe, Ca and Cu. The intensities of the x-ray diffraction lines for these compounds is the largest for the ROFA samples obtained from the high sulfur No. 6 oil and for the $PM_{2.5}$ fraction of No. 5 oil (BL5FH). This is understandable since the high sulfur content would tend to produce higher levels of the sulfates. The other noticeable trend is the higher concentrations of the sulfates in the $PM_{2.5}$ fraction as compared to the $PM_{2.5+}$ fraction.

The major contribution of the present investigation using x-ray diffraction is that we have been able to identify various compounds and their water content in the ROFA samples. In making the identifications, we compared the diffraction patterns of all appropriate compounds available in the JCPDS files. Since the studies by Miller et al [7] had given the percentages of various elements present in these samples, our search was primarily confined to the various compounds of these elements. The information reported here on the various compounds should be useful for developing appropriate models for the formation of these compounds. Some of these compounds may have appropriate band gaps for the photocatalytic absorption of solar radiation [9]. In addition, some of these materials being acidic, may have the catalytic ability to crack hydrocarbons and create free radicals. Further work along these lines is needed to understand the harmful effects of $PM_{2.5}$. A more detailed description of our

investigations, including comparison with the findings obtained by other techniques, will be published elsewhere.

ACKNOWLEDGEMENT

Support of this research under the U.S. Department of Energy contract No. DE-AC26-99BC15220 is gratefully acknowledged. We thank Dr. G. P. Huffman for providing the samples used in these investigations.

REFERENCES

1. Federal Register, 62 FR 38652, July 18, 1997.
2. D. W. Dockery, C. A. Pope, X. Xu, J. D. Spengler, J. H Ware, M. E. Fay, B. G. Ferris, and F. E. Speizer, New England J. Med., 329 (1993) 1753.
3. R. T. Burnet, R. Dales, D. Krewski, R. Vincent, T. Dann, and J. R. Brook, Am. J. Epidemiology, 142 (1995) 15.
4. J. Schwartz, and R. Morris, Am. J. Epidemiology, 142, (1995) 23.
5. Chemical Engineering News, Particulate matter health studies to be reanalyzed August 18, (1997) 33.
6. G. P. Huffman, F. E. Huggins, R. E. Huggins, W. P. Linak and C. A. Miller, Proc. Pittsburgh Coal Conf. 1999 (to be published).
7. C. A. Miller, W. P. Liank, and J. O. L. Wendt, Proceedings, Conf. On Air Quality, Dec. 1-4, 1998; to be published in Fuel Processing Technology.
8. V. S. Babu, L. Farinash and M. S. Seehra, J. Mater. Res., 10, 1075 (1995).
9. R. R. Chianelli, Synthesis, fundamental properties and applications of nanocrystals, sheets, and fullerenes based on layered transition metalchalcogenides. In R&D status and trends, ed. Siegel et al. (1998).

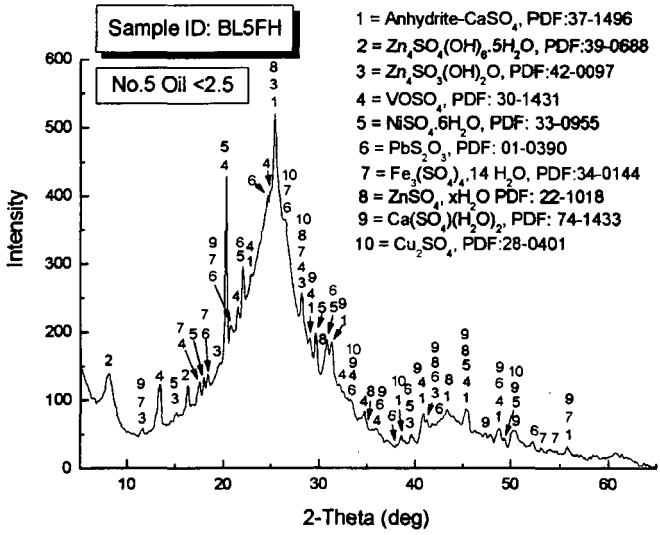

Fig. 1 Room temperature x-ray diffractogram of sample BL5FH. Lines due to various crystalline components are identified.

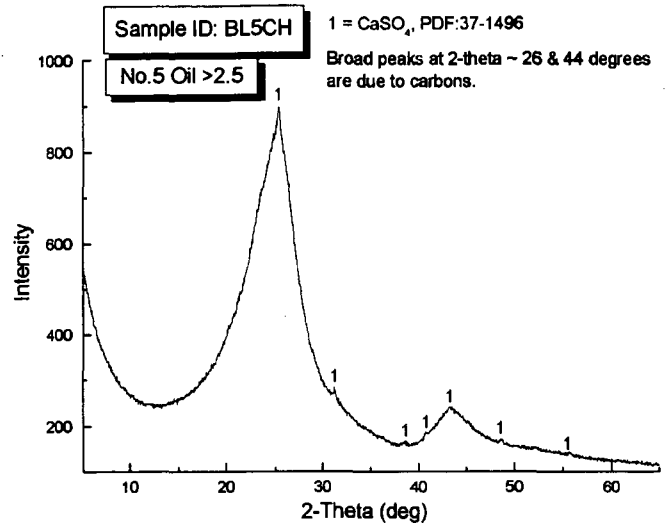

Fig. 2 Room temperature x-ray diffractogram of sample BL5CH. Lines only due to $CaSO_4$ are present. The broad peaks near $2\theta \sim 26°$ and 44° are due to amorphous carbons (see Ref. 8).

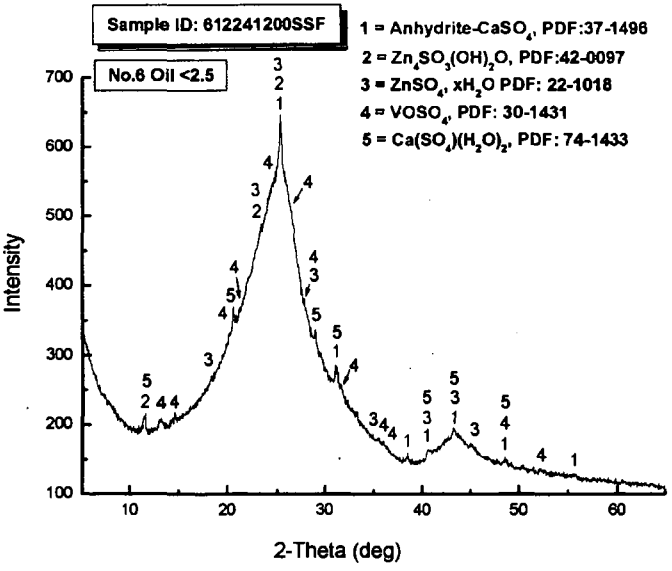

Fig. 3 Room temperature x-ray diffractogram of sample 612241200SSF. Lines due to various crystalline components are identified. The broad peaks are due to amorphous carbon.

Table 1: Identification of the compounds in the ROFA samples

Sample	Compound (PDF File)
BL5FH (#5 oil) <2.5	$CaSO_4$ (37-1496); $Zn_4SO_4(OH)6.5H_2O$ (39-0688); $Zn(SO_3).2.5H_2O$ (42-0097); $VOSO_4$ (30-1431); $NiSO_4.6H_2O$ (33-0955); PbS_2O_3 (01-0390); $Fe_3(SO_4)_4.14H_2O$ (34-0144); $ZnSO_4xH_2O$ (22-1018); $Ca(SO_4)(H_2O)_2$ (74-1433); Cu_2SO_4 (28-0401)
BL5CH (#5 oil) >2.5	$CaSO_4$ (37-1496)
701291400SSF (#6 oil) high sulfur <2.5	Same as BL5FH
70129400SSC (#6 oil) high sulfur >2.5	Same as BL5FH
612241200SSC (#6 oil) medium sulfur >2.5	$CaSO_4$ (37-1496); $Zn(SO_3).2.5H_2O$ (42-0097); $Ca(SO_4)(H_2O)_2$ (74-1433)
612241200SSF (#6 oil) medium sulfur <2.5	$CaSO_4$ (37-1496); $Zn(SO_3).2.5H_2O$ (42-0097); $ZnSO_4xH_2O$ (22-1018); $VOSO_4$ (30-1431); $Ca(SO_4)(H_2O)_2$ (74-1433)
701071200SSF (#6 oil) low sulfur <2.5	$CaSO_4$ (37-1496); $Zn(SO_3).2.5H_2O$ (42-0097); $VOSO_4$ $1.5H_2O$ (31-1444); $NiSO_4$ (34-0144); $Ca(SO_4)(H_2O)_2$ (74-1433)
807161300SSF baseline filter	$CaSO_4$ (37-1496); $VOSO_4$ (30-1431); $NiSO_4.6H_2O$ (33-0955); PbS_2O_3 (01-0390); $Fe(NO_3)_3.9H_2O$ (01-0124); $ZnSO_4xH_2O$ (22-1018); $Ca(SO_4)(H_2O)_2$ (74-1433); Cu_2SO_4 (28-0401); $NaAl(SO_4)_2.6H_2O$ (19-1186)

XAFS Spectroscopy and SEM Investigation of Fine Particulate Matter from Residual Fuel Oil Combustion

G. P. Huffman*, F. E. Huggins*, R. Huggins*, W. P. Linak+, C. A. Miller+, R. J. Pugmire# and H. L. C. Meuzelaar#,
*University of Kentucky, 533 S. Limestone St. – Rm.111, Lexington, KY 40506
+U.S. Environmental Protection Agency, National Risk Management Research Laboratory, Research Triangle Park, NC 27711
Dept. of Chemical and Fuels Engineering, University of Utah, Salt Lake City, Utah

Keywords: particulate matter, $PM_{2.5}$, XAFS, NMR, molecular structure, SEM, particle size distribution

Introduction

The EPA is currently considering new regulations for fine airborne particulate matter (PM) less than 2.5 microns in diameter ($PM_{2.5}$). Such regulations should be based on the best scientific data, particularly with regard to fine particle characterization. Although there are many analytical techniques for determining the elemental composition of $PM_{2.5}$, information on molecular speciation is much more difficult to obtain. Since the health effects of $PM_{2.5}$ are closely related to speciation parameters such as valence, solubility and acidity, it is essential to identify and evaluate analytical methods that can accurately speciate the molecular structure of critical elements.

X-ray absorption fine structure (XAFS) spectroscopy is a synchrotron radiation – based technique that is uniquely well suited to characterization of the molecular structure of individual elements in complex materials. In previous research, we have used XAFS spectroscopy to determine the molecular forms of environmentally important elements (S, Cl, As, Cr, Hg, Ni, etc.) in coal, oil, flyash, and sorbents.[1-7] Our initial investigations of PM indicate that XAFS will also be a powerful tool in this area.[8,9]

In the current work, XAFS spectroscopy was used to investigate several elements in a suite of residual oil flyash (ROFA) samples separated aerodynamically into fractions <2.5 ($PM_{2.5}$) and >2.5 microns ($PM_{2.5+}$) in diameter. The ROFA was generated by combustion of residual fuel oil at the EPA National Risk Management Laboratory.[10] Complementary data were obtained using computer-controlled scanning electron microscopy (CCSEM), ^{13}C NMR, GC/MS, and XRD. In the current paper, some examples of the XAFS, CCSEM, and NMR data are presented. The XRD data are discussed in a separate paper presented in this symposium by Seehra and Mannivanan.[11]

Experimental Procedure

The combustion experiments were carried out in a North American three-pass fire tube package boiler, which is a practical, commercially available heavy fuel oil combustion unit. A detailed description of this boiler is given elsewhere.[10] Samples were separated aerodynamically by a cyclone into $PM_{2.5}$ and $PM_{2.5+}$ fractions. The sampling system consists of a large dilution sampler capable of isokinetically sampling 0.28 m^3/min (10 ft^3/min) of flue gas using a Source Assessment Sampling System (SASS) cyclone. The SASS cyclone produces 50 and 95% collection efficiencies at approximately 1.8 and 2.5 micron diameter, respectively. The resulting PM is collected on large (65 cm) Teflon coated glass fiber filters, transferred to sampling jars, and made available for analysis.

Although burnout was fairly complete (>99.7 %), the inorganic content of the oils was quite low (0.02-0.10 wt.% ash), and the dominant element of the ROFA is carbon. Loss on ignition (LOI) measurements indicates that the carbon content of the $PM_{2.5}$ ranged from 64 to 87 wt.% and that of the $PM_{2.5+}$ from 88 to 97 wt.%. S content of the PM samples was ~ 1 to several wt.%, while the V content ranged from 0.5 to 5.9 wt.%, and the Ni content from 0.08 to 0.8 wt.%. The metals are typically more concentrated in the $PM_{2.5}$ samples than they are in the $PM_{2.5+}$ samples by factors ~3 to 6.[10]

The samples were investigated by XAFS spectroscopy at the Stanford Synchrotron Radiation Laboratory (SSRL) and the National Synchrotron Light Source (NSLS) at Brookhaven National Laboratory. All measurements were carried out in the fluorescent mode using either a Lytle detector or a multi-element Ge array detector, as described

elsewhere.[1-4] The XANES regions of the spectra were analyzed by deconvolution, derivative, and comparative analysis methods, as discussed in earlier papers.[1-7]

Results and Discussion

CCSEM examination of the $PM_{2.5}$ was carried out on samples dispersed on a nucleopore filter, prepared as discussed elsewhere.[12] Since the particles were predominantly carbon rich, C was by far the dominant element detected in the energy dispersive x-ray (EDX) spectra. S, V and Ni were observed as minor components. Because the sample contained both a large particle component and a small particle component, quantitative particle size distributions have not yet been obtained. However, measurements of the spread of the PSD were obtained by examining fields containing primarily small particles at magnifications ~1000X and fields containing large particles at a magnification of 50X. Examples are shown in Figure 1. It is seen that the PSD of the small particle component peaks at 1-3 microns and that of the large particle component at 10-15 microns.

Typical S K-edge XANES spectra of ROFA $PM_{2.5}$ and $PM_{2.5+}$ samples are shown in Figure 2. The spectra are deconvoluted by a least squares computer analysis into a series of peaks (50% Lorentzian-50% Gaussian) and two rounded arctangent step functions, as discussed elsewhere.[1,2] Most of the peaks represent $1s \rightarrow 3p$ transitions of photoelectrons excited from the K-shell by x-ray absorption. Both the position and relative intensity of these peaks vary significantly with the electronic state of the S atom, increasing with increasing valence. By using calibration data generated from mixtures of standard compounds, the peak area percentages can be translated into percentages of S contained in different molecular forms.[1,2]

The results of this analysis for the ROFA PM samples are summarized in Table 1. For comparison, the results for the PM derived from combustion of a Pittsburgh No. 8 coal in the same boiler are also included. The dominant molecular forms of S observed are sulfate and thiophenic S. Sulfate was greater in the $PM_{2.5}$ samples than in the $PM_{2.5+}$ samples, reflecting the greater degree of carbon burnout for the smaller particles. Additional components, including elemental S and inorganic sulfides, are present in lower percentages. The origin of the elemental S is not clear at this time. The S in the $PM_{2.5}$ of the ROFA from a high S residual oil burned in a second furnace where carbon burnout was much more complete was 100% sulfate. It is seen that both the $PM_{2.5}$ and $PM_{2.5+}$ from the Pittsburgh #8 coal are also predominantly sulfate.

Table 1. XANES results for the weight percentages of different S forms.

Sample	PM size	Sulfate	Thiophene	Elemental S	Inorganic sulfide	Other forms
Baseline # 5 oil	< 2.5	55	24	5	11	5
Baseline # 5 oil	>2.5	32	37	8	19	4
Low S #6 oil	< 2.5	84	14	--	--	2
Low S #6 oil	>2.5	58	34	6	--	2
Med. S #6 oil	< 2.5	73	13	6	--	8
Med. S #6 oil	>2.5	55	35	6	--	3
High S #6 oil	< 2.5	54	29	5	11	1
High S #6 oil	>2.5	26	39	9	26	--
Pitt. #8 coal	< 2.5	95	5	--	--	--
Pitt. #8 coal	>2.5	85	14	--	--	1

Analysis of the XANES spectra from V and Ni in the ROFA PM samples indicates that they are present predominantly as sulfates. Most of the V XANES spectra closely resemble the spectrum of vanadyl sulfate ($VO{\cdot}SO_4{\cdot}xH_2O$). This is brought out clearly by the first derivative of the XANES spectra, which exhibited peaks in nearly identical positions and with similar intensities to the first derivative of the XANES spectrum of $VO{\cdot}SO_4{\cdot}3H_2O$ reported by Wong et al.[12] The Ni XANES and first derivative spectra from the PM samples agree well with that of $NiSO_4$, and with the Ni spectra observed in an earlier investigation of ROFA[4] by the current authors. Similarly, the XANES and the

first derivative spectra of the other metals examined (Fe, Zn, Cu, Mn and Pb) also identify the principal components of these metals to be sulfates. However, secondary components are present in many of the metal XAFS spectra. In most cases, these secondary components appear to be oxides. The As XANES identify the arsenic as an arsenate (As^{+5}) but do not identify the specific phase.

NMR data

Seven of the samples were examined by ^{13}C NMR. Cross polarization experiments suggested that the proton content of the samples was very low and, hence, no useful data were obtained using this experimental technique. Proton spectra taken on several samples verified the very low H/C ratios for all but the high sulfur #6 $PM_{2.5}$ sample. The ^{13}C NMR spectra were then acquired using by using block decay with a pulse repetition rate of 10 s and accumulating between 17,000 and 25,000 scans. These resulting spectra are shown in Figure 3, where FL and CY denote filter ($PM_{2.5}$) and cyclone ($PM_{2.5+}$) samples, HS, MS and LS indicate high, medium and low sulfur #6 oil, and BL indicates baseline #5 oil. The spectra indicate that the carbon in the samples is predominantly condensed in graphitic-like structures. Second moment (line width) measurements are uniform at ~75 ppm (FW/HH) for six of the samples. However, the second moment of the high sulfur #6 $PM_{2.5}$ (FL-HS) sample indicates a much narrower aromatic band (45 ppm). In addition, this sample is unique in that aliphatic structure is clearly present in the spectrum.

Summary and Conclusions

XAFS spectroscopy, CCSEM and ^{13}C NMR data have been obtained from a series of $PM_{2.5}$ and $PM_{2.5+}$ samples produced by combustion of residual fuel oil in a commercial boiler. Analyses of the XANES spectra have been carried out for S and a number of metals in the PM. Deconvolution of the S XANES reveals that the dominant molecular forms of S observed are sulfate and thiophenic S. Sulfate was greater in $PM_{2.5}$ samples than in the $PM_{2.5+}$ samples, reflecting the greater degree of carbon burnout for the smaller particles. Sulfates are the dominant components of the metal spectra. CCSEM indicates that the aerodynamically separated $PM_{2.5}$ is bimodal in size, with a small particle component peaking at 1-3 microns and a large particle component peaking at 10-15 microns. The ^{13}C NMR indicated that the carbon in the PM was predominantly graphitic or soot-like in structure. However, one sample exhibited a much narrower aromatic band than the others and an aliphatic component.

Acknowledgement: Support of this research under U.S. Department of Energy (FE/NPTO) contract No. DE-AC26-99BC15220 is gratefully acknowledged. The XAFS experiments were conducted at the Stanford Synchrotron Radiation Laboratory and the National Synchrotron Light Source, which are also supported by the U.S. DOE.

References:

1. G.P. Huffman, S. Mitra, F.E. Huggins, N. Shah, S.Vaidya, and F. Lu, **1991**, *Energy & Fuels*, **5**, 574-581.
2. M.Mehdi Taghiei, F.E. Huggins, N. Shah, and G.P. Huffman, **1992**, *Energy & Fuels*, **6**, 293-300.
3. G.P. Huffman, F.E. Huggins, N. Shah, and J. Zhao, **1994**, *Fuel Processing Technology*, **39**, 47-62.
4. F.E. Huggins and G.P. Huffman, **1996**, *Int. J. Coal Geology*, **32**, 31-53.
5. K.C. Galbreath, C.J. Zygarlicke, D.L. Toman, F.E. Huggins and G.P. Huffman, **1998**, *Energy & Fuels*, **12(4)**, 818-822.
6. F.E. Huggins, M. Najih, and G.P. Huffman, **1999**, *Fuel*, **78**, 233-242.
7. F.E. Huggins, G. P. Huffman, G. E. Dunham, and C. L. Senior, **1999**, *Energy & Fuels*, **13**, 114-121.
8. F.E. Huggins, G.P. Huffman, and J. David Robertson, ACS, Div. Environ. Chem., Preprints, 1998, **38(2)**.
9. F. E. Huggins and G. P. Huffman, **1999**, *J. of Hazardous Materials*, in press.
10. C. A. Miller, W. P. Linak, C. King, and J. O. L. Wendt, **1998**, *Combust. Sci. and Technol.*, **134**, 477-502.
11. M.S. Seehra and A. Mannivannan, this volume.
12. G. Huffman, A. Shah, N. Shah J. Zhao, F. Huggins, J. Helble, S. Srinivasachar, T. Peterson, J. Wendt, N. Gallagher, L. Bool, A. Sarofim, Proc. Eng. Fd. Conf., The Impact of Ash Deposition on Coal Fired Plants, Eds., J. Williamson and F. Wigley, **1994**, pp. 409-423, Taylor & Francis, London.

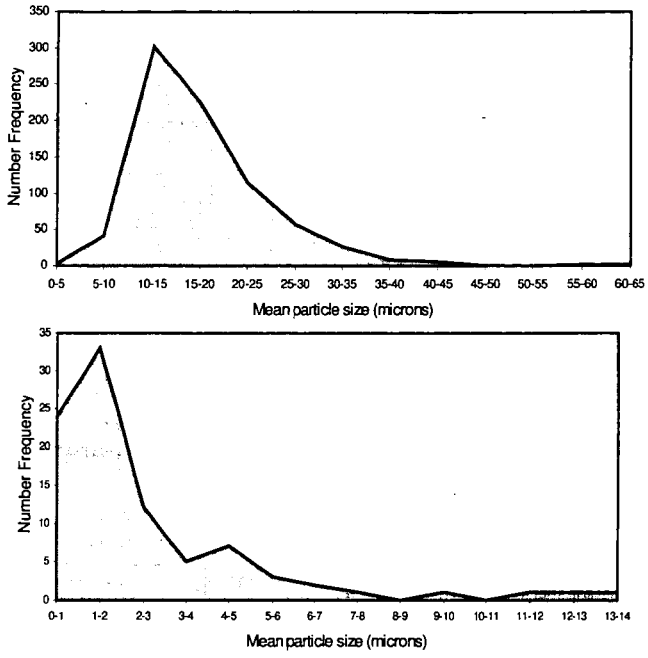

Figure 1. Particle size distributions for $PM_{2.5}$ measured for a field of particles at a magnification of 50X and a second field at a magnification of 1000X.

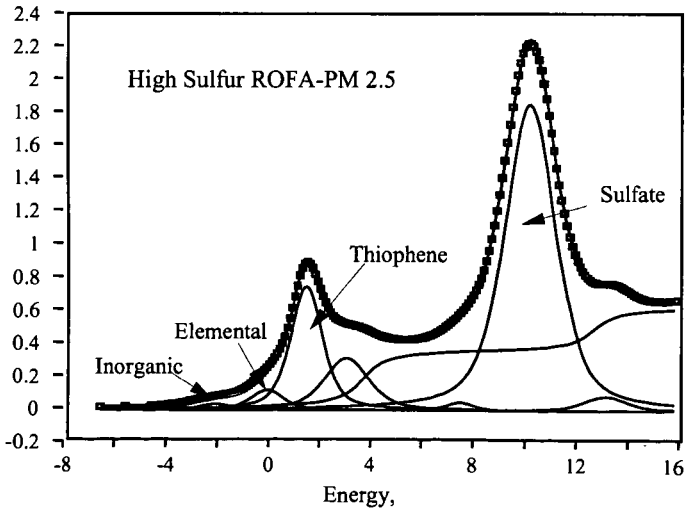

Figure 2. Typical least squares analysis of the S XANES of a ROFA $PM_{2.5}$ sample.

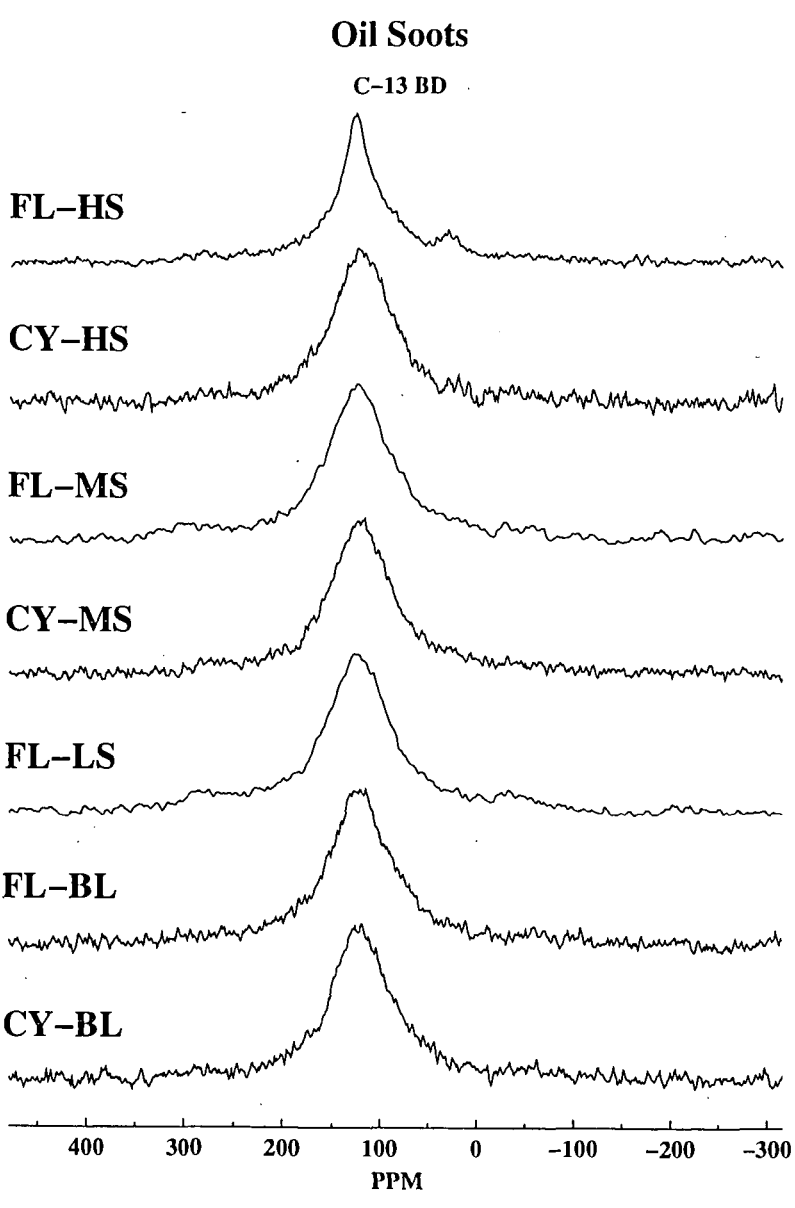

Figure 3. ^{13}C NMR Spectra of ROFA PM Samples.

SUPER-EQUILIBRIUM CONCENTRATIONS OF CARBON MONOXIDE AND HYDROCARBON IN FUEL GASES AND THEIR RELATIONASHIP WITH VOC AND METALS EMISSIONS

Alan Williams, Andy Ross, Suparin Chaiklangmuang,
Jenny M Jones, and Mohammed Pourkashanian.

Department of Fuel & Energy,
Leeds University, Leeds, LS2 9JT, United Kingdom.

KEYWORDS: Coal combustion; Emissions of CO, VOC, PAH, trace metal; modelling

INTRODUCTION

Flue gases resulting from the combustion of hydrocarbon fuels in practical systems usually contain levels of carbon monoxide that are significantly above equilibrium values. Typically, for flue gases from a utility plant containing 5% O_2, the measured level of carbon monoxide is about 300 ppm. The computed equilibrium value is extremely small with 3% O_2 and rises rapidly as the O_2 level is reduced. If combustion took place in the combustion chamber with perfectly-mixed fuel and combustion air, the lower levels of carbon monoxide would result. However, mixing is not perfect because of the formation of coherent structures and large turbulent eddies. These unburned pockets of rich mixtures are caused by incomplete mixing of fuel and air at the near-burner zone, and persist because of the slow subsequent mixing with air. They are responsible for the above equilibrium levels of hydrocarbons, namely the volatile organic compounds (VOC) found in the flue gases.

The super-equilibrium levels of carbon monoxide can also be responsible for corrosion cracking in earlier parts of certain boilers, is related to the presence of unburned hydrocarbons, and can have some influence on the chemistry of the metals emitted. In this paper, values of the super-equilibrium levels of carbon monoxide and VOC's are computed together with their influence on metal emission.

A similar situation can hold for smoke where the concentrations in the rich pocket are above those expected for a uniformly mixed gas. These higher local soot concentrations can coagulate faster and can result in sub-micron particulate matter even in lean mixtures.

EXPERIMENTAL

Thermodynamic equilibrium concentrations of major VOCs, certain polycyclic aromatic hydrocarbons (PAHs) and trace element species were determined by means of minimisation of free energy calculations using "Equitherm" (VCH scientific Software, Equitherm version 5.0).[1] The calculations presented here were designed to determine the effect of carbon monoxide levels on species for arsenic, chorine, cadmium, mercury, nickel, lead and thallium. The system examined uses a sub-stoichiometric basis and calculates the formation of all gaseous, liquid and solid phase species at 1 atm. pressure over a range of temperatures (500 - 1800 K), and amount of air supplied (300, 250, 200 and 150 kg corresponding to between approximately ¼ to ⅛ of stoichiometric air) and is based on 100 kg of coal. Two coals with very different properties were investigated, Thai coal and Pittsburgh #8 coal, and the analyses of which are given in Table 1.

RESULTS AND DISCUSSION

Equilibrium predictions of CO concentrations are low compared to CO_2. However, actual CO concentrations in flue gases are much higher than equilibrium values. These higher CO concentrations could arise from poor mixing in the combustion system, resulting in a drastic decrease in local O_2 concentrations, and consequently increases in CO concentration. Such a situation could be described by the formation of fuel-rich turbulent eddies, which mix, and therefore cool, relatively slowly. Within these fuel rich pockets, reactions of volatile gases, fuel and unburned or partially oxidised species take place in an oxygen deficient atmosphere. Figure 1 describes the change in CO, CH_4 and C_6H_6 concentration at 1500 K as the air supply is varied. A rapid increase in CO between 300 and 250 kg air (per 100 kg fuel) is observed. As the mixture becomes richer, benzene and methane also start to increase in concentration,

Table 1 Summary of characterisation analysis on original coal sample

	Thai coal		Pittsburgh #8	
	As determined (wt%)	Dry basis (wt%)	As determined (wt%)	Dry basis (wt%)
% ash	25.43	22.54	9.84	9.68
%carbon	56.45	50.04	74.66	73.45
%hydrocarbon	13	11.52	5.2	5.12
%nitrogen	1.69	1.50	1.7	1.67
%oxygen (difference)	3.43	3.04	8.6	8.46
%sulfur	1.98	1.76	2.19	2.15
%moisture	12.81		1.65	
concentration of metal in ppm, wt.				
As	11.28	10.0	3.36	3.31
Cd	0.56	0.5	0.03	0.029
Ni	22.56	20.0	1.70	1.67
Pb	45.12	40.0	1.85	1.82
Tl	1.13	1.0	1.02	1.0
Hg	0.11	0.1	0.12	0.12
Cl	1128.10	1000.0	0.12	0.12
kJ/kg	27110	24030	31960	31440

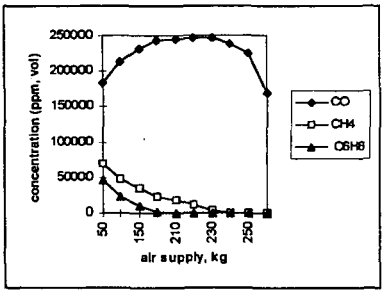

Fig 1: Thermodynamic prediction of the equilibrium concentration of CO, CH_4 and C_6H_6 at 1500K

and CO begins to decrease. If calculations are performed at leaner conditions (up to 600 kg air) the CO concentration decreases to very low levels, as do the VOC species.

Figure 2 indicates the concentration profiles with temperature of hydrocarbons at both 150 and 300kg air /100kg coal. Equilibrium conditions are not expected to be attained at lower temperature in the reaction times available.[2] Transient kinetic calculations indicate that the equilibrium concentrations produced at high temperature (i.e. above ~ 1273 K) are reasonable, but that the species are quenched as the rich pockets cool. The window of stability for hydrocarbons is related to O_2 concentration. Concentrations of the larger polyaromatic hydrocarbons (PAH) ($C_{10}H_8$ and $C_{20}H_{12}$) are predicted to rise rapidly at lower O_2 concentrations. The increased concentration of PAH and other reduced species results in the increased probability of soot formation and agglomeration, through collision and reaction in the rich turbulent eddies.

Throughout the temperature range studied (500-1800K) the distribution of metals can be followed as shown in Figure 3a and 3b for Pittsburgh coal. The concentration of air affects the overall distribution of the metals between the solid and gas phase. The reduction in air also influences the speciation of the metals causing many of them to be fixed in the solid phase up to a higher temperature. The presence of fuel rich "pockets" in the combustion system appears to be beneficial for many trace metals, because the formation of solid chlorides and sulphides is favoured at higher temperatures for richer pockets. E.g. for 300 kg air, the transformation of cadmium occurs in the temperature range 900 - 1000 K corresponding to the transformation of Cd metal (g) to CdS (s). A slight increase in $CdCl_2$ effects the distribution of cadmium. For lead, solidification of PbS vapour is expected to be independent of air concentration, and occurs at 700-800 K. The temperature for partitioning of thallium between gas and solid phases is changed slightly by changing the air concentration. In terms

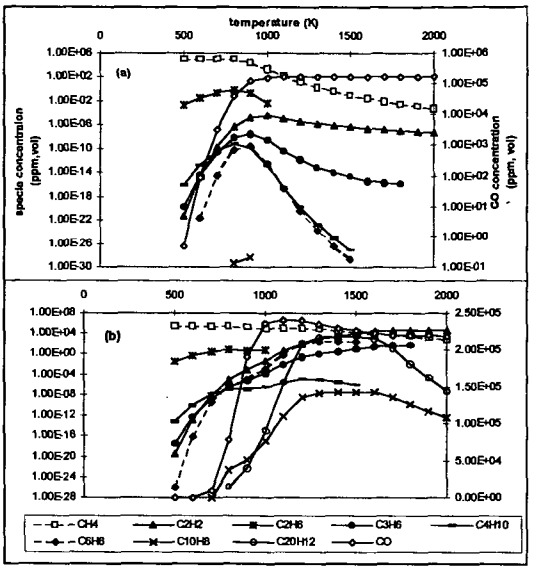

Fig 2: Thermodynamic prediction of equilibrium concentrations of gases for Thai coal: at (a) air 300 kg, and (b) air 150 kg.

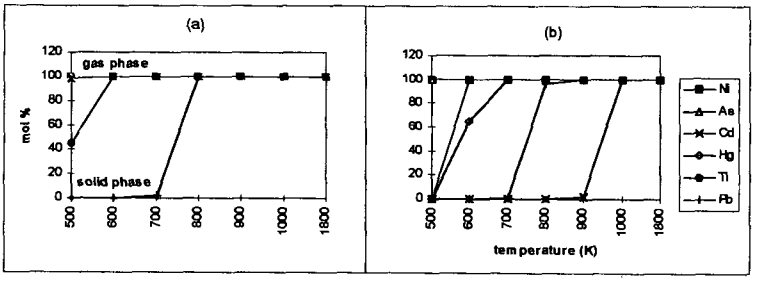

Fig 3: (a) Distribution of metal species in fuel gas and ash for Pittsburgh coal: (a) air 300 kg (b) air 200 kg

of distribution between the phases, Hg remains in the gas phase throughout the temperature range for 300 kg air/100kg fuel (Fig. 3a) predominantly as Hg (metal). At leaner conditions (Fig. 3b) mercury is in the gas phase as HgS (g), which forms a solid phase at low temperatures.

Ni and As are present in the gas phase even at low temperatures regardless of air concentration. Ni is released as $Ni(CO)_4$ and appears to independent of air concentration. Even at stoichiometric air (or above), nickel carbonyl is predicted to be the most stable nickel species. Figure 4 shows the distribution of metal speciation for nickel. The higher emission for the Thai coal simply reflects the higher concentration of nickel in the original coal.

Arsenic on the other hand is very sensitive to the air concentration, as shown in Figure 5. At 350 kg air, the arsenic is predominantly AsO(g) over the entire temperature range. However at 300 kg air, higher temperature favours the decomposition of AsO(g) and the formation of the highly toxic hydride, arsene (AsH_3).

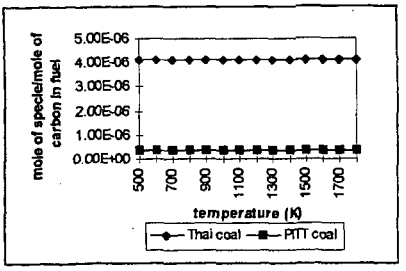

Fig 4: Equilibrium concentration of $Ni(CO)_4$ for Thai coal and Pittsburgh coal with 300kg air/100kg coal

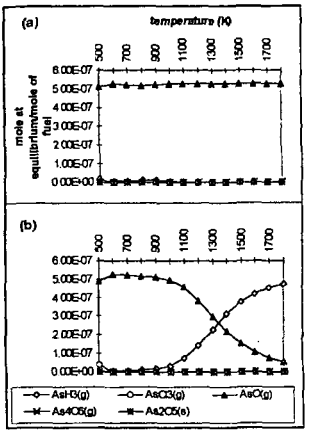

Fig 5: Equilibrium distribution of Arsenic species at 350 (a) and 300 (b) kg of air for *Pittsburgh #8* coal.

CONCLUSIONS

One route to the emission of VOC and PAH from combustion processes is via the formation of fuel-rich turbulent eddies in the flame. The local gaseous environment in these eddies favours the formation of super-equilibrium concentrations of all organic species. The concentration of CO may be used as a marker to calculate emissions of organic species, since a direct correlation is observed, although the nature of the fuel also influences the relative concentrations.

Trace metals, present in the fuel-rich "pockets", are predicted to change their speciation behaviour, compared to a fuel-lean situation. In some cases the thermodynamics acts in favour of decreasing the flue gas emission factor of the metal in question (e.g. thallium). However, the predictions for the influence on the emission of certain metal species (e.g. nickel and arsenic) is of concern. Possible routes to nickel carbonyl and arsene (AsH_3) are apparent.

AKCKNOWLEDGEMENTS

The authors would like to express their appreciation to the Thai Government for financial assistance of Ms S Chaiklangmuang through a PhD studentship.

REFERENCES

1. H.K.Chagger, J.M.Jones, M.Pourkashanian and A.Williams; Fuel, 1997, 76, 9, 864.
2. Barin, I., Thermochemical Data of Pure substances, 2nd edn. VCH, Weinheim, 1992.

FIELD TESTING OF THE ADVANCED HYBRID PARTICULATE COLLECTOR, A NEW CONCEPT FOR FINE-PARTICLE CONTROL

Stanley Miller (smiller@eerc.und.nodak.edu, [701] 777-5210)
Michael Jones (mjones@eerc.und.nodak.edu, [701] 777-5152)
Energy & Environmental Research Center

Kenneth Walker (kwalker@wlgore.com, [410] 506-3300)
Richard Gebert (rgebert@wlgore.com, [410] 506-3218)
John Darrow (jdarrow@wlgore.com, [410] 506-3316)
W.L. Gore & Associates, Inc.

Dr. Henry Krigmont (alentec@alentecinc.com, [714] 799-9895)
Allied Environmental Technologies Company

Thomas Feeley (feeley@fetc.doe.gov, [412] 386-6134)
U.S. Department of Energy

William Swanson (wswanson@otpco.com, [605] 862-8125)
Otter Tail Power Company

KEYWORDS: Fine-particle control and coal-fired boiler

INTRODUCTION

A new concept in particulate control, called an advanced hybrid particulate collector (AHPC), is being developed at the Energy & Environmental Research Center (EERC) with U.S. Department of Energy (DOE) funding. In addition to DOE and the EERC, the project team includes W.L. Gore & Associates, Inc., Allied Environmental Technologies, Inc., and the Big Stone power station (jointly owned by three partners: Northwestern, Montana–Dakota Utilities, and Otter Tail Power Company.) The AHPC combines the best features of electrostatic precipitators (ESPs) and baghouses in a unique approach to develop a compact but highly efficient system. Filtration and electrostatics are employed in the same housing, providing major synergism between the two collection methods, both in the particulate collection step and in the transfer of dust to the hopper. The AHPC provides ultrahigh collection efficiency, overcoming the problem of excessive fine-particle emissions with conventional ESPs, and solves the problem of reentrainment and re-collection of dust in conventional baghouses.

The goals for the AHPC are as follows: >99.99% particulate collection efficiency for particle sizes from 0.01 to 50 μm, applicable for use with all U.S. coals, and cost savings compared to existing technologies.

The electrostatic and filtration zones are oriented to maximize fine-particle collection and minimize pressure drop. Ultrahigh fine-particle collection is achieved by removing over 90% of the dust before it reaches the fabric and using a GORE-TEX® membrane fabric to collect the particles that reach the filtration surface. Charge on the particles also enhances collection and minimizes pressure drop, since charged particles tend to form a more porous dust cake. The goal is to employ only enough ESP plate area to precollect approximately 90% of the dust. ESP models predict that 90% to 95% collection efficiency can be achieved with full-scale precipitators with a specific collection area (SCA) of less than 100 ft^2/kacfm [1]. Fabric filter models predict that face velocities greater than 12 ft/min are possible if some of the dust is precollected and the bags can be adequateiy cleaned. The challenge is to operate at an air-to-cloth (A/C) ratio of 12 ft/min or greater for economic benefits while achieving ultrahigh collection efficiency and controlling pressure drop. The combination of GORE-TEX® membrane filter media, small SCA, high A/C ratio, and unique geometry meets this challenge.

Studies have shown that fabric filter collection efficiency is likely to deteriorate significantly when the face velocity is increased [2, 3]. For high collection efficiency, the pores in the filter media must be effectively bridged (assuming they are larger than the average particle size). With conventional fabrics at low A/C ratios, the residual dust cake serves as part of the collection media, but at high A/C ratios, only a very light residual dust cake is acceptable, so the cake cannot be relied on to achieve high collection efficiency. The solution is to employ a sophisticated fabric that can ensure ultrahigh collection efficiency and endure frequent high-energy cleaning. In addition, the fabric should be reliable under the most severe chemical environment likely to be encountered (such as high SO_3). A fabric that meets these requirements

is GORE-TEX® membrane on GORE-TEX® felt. GORE-TEX® membrane filter bags consist of a microporous, expanded polytetrafluoroethylene (PTFE) membrane laminated to a felted or fabric backing material. Consequently, even fine, nonagglomerating particles do not penetrate the filter, resulting in significant improvements in filtration efficiency, especially for submicron particles. This fabric is also rugged enough to hold up under rigorous cleaning, and the all-PTFE construction alleviates concern over chemical attack under the most severe chemical environments.

Assuming that low particulate emissions can be maintained through the use of advanced filter materials and that 90% of the dust is precollected, operation at face velocities in the range from 12–24 ft/min should be possible, as long as the dust can be effectively removed from the bags and transferred to the hopper without significant redispersion and re-collection. With pulse-jet cleaning, heavy residual dust cakes are not typically a problem because of the fairly high cleaning energy that can be employed. However, the high cleaning energy can lead to significant redispersion of the dust and subsequent re-collection on the bags. The combination of a very high-energy pulse and a very light dust cake tends to make the problem of redispersion much worse. The barrier that limits operation at high A/C ratios is not so much the dislodging of dust from the bags as it is transferring the dislodged dust to the hopper. The AHPC achieves enhanced bag cleaning by employing electrostatic effects to precollect a significant portion of the dust and by trapping in the electrostatic zone the redispersed dust that comes off the bags following pulsing.

CONCEPT DEVELOPMENT AND FIELD TESTING

Phase I of the development effort consisted of design, construction, and testing of a 200-acfm working AHPC model [4, 5]. Since all of the developmental goals of Phase I were met, the approach was scaled up in Phase II to a size of 9000 acfm and installed at the Big Stone power station (see specification in Table 1 and top view in Figure 1).

Big Stone power plant was commissioned for service in 1975. The unit is a 450-MW-rated, Babcock and Wilcox cyclone-fired boiler. The primary fuel for the first 20 years of operation was North Dakota lignite, but four years ago, the primary fuel was switched to Powder River Basin subbituminous coal. This fuel has approximately one-half of the moisture and one-third more heat than North Dakota lignite. Almost all of the effects of this new fuel have been positive. However, one challenge that has occurred is the decreased efficiency of the ESP, due to an increase in resistivity of the fly ash. The combination of a very fine particle size produced from the cyclone-fired boiler and high ash resistivity make this a challenging test dust for the AHPC.

After completing the shakedown testing, the field AHPC unit was started on July 29, 1999. Based on shakedown testing, the initial secondary current was set at 50 mA and the bag cleaning trigger point was set at 8 in. W.C. to initiate pulsing all four rows of bags in sequence. The flow rate was set to a nominal 12 ft/min based on pitot readings. However, since the fan speed was not automatically controlled by the flow rate, there was always an increase in flow rate after pulsing. With the increase in flow after pulsing, the integrated average flow rate throughout the pulsing cycles was typically in the range from 12 to 13 ft/min during the first 6-week test period.

Over the course of the first 6 weeks, there were a number of interruptions to the operation. During this time, there were six unplanned outages to the plant ranging from a few hours up to 24 hours. In each case, the outage caused the induced-draft (ID) fan to shut down automatically, and the AHPC was then brought on-line manually when the plant was up to stable operating conditions. There were also two occurrences where significant rainfall led to water leaking into the AHPC around an insulator, which resulted in arcing and automatic shutdown of the ESP power supply. In these cases, the AHPC remained on-line, but the pulse interval increased significantly without ESP power.

While the multiple unplanned outages added difficulty to the AHPC operation, they also provided a severe test of the ruggedness of the AHPC during multiple start-ups, power outages, and moisture in the compartment. In spite of all of these interruptions, the AHPC continued to operate with a reasonable pulse-cleaning interval in the range from 10–30 minutes.

Two inlet and two outlet U.S. Environmental Protection Agency (EPA) Method 17 dust loadings were completed after 3 weeks of operation (see Table 2). Based on these measurements, the collection efficiency was at least 99.99%. However, the measured efficiency was somewhat limited by the weighing accuracy of the filters before and after sampling. The sampling time for the second outlet dust loading was extended to 17 hours to lower the detection limit. The ultrahigh collection efficiency was confirmed by the perfectly clean outlet filter, even after

sampling for 17 hours. The flue gas moisture values of 12% along with leak checks of the sampling trains before and after sampling provide quality control checks that the indicated flue gas volume was the actual volume sampled. Another indication of ultrahigh collection is that inspection of the clean plenum area of the AHPC following 6 weeks of operation showed the tube sheet to be completely clean.

Since the dust is known to cause operational difficulties for the Big Stone ESP because of high resistivity, it was expected that resistivity problems might also be an issue with the AHPC. Significant sparking and back corona were present from the first days of operation. Visual inspection through the sight ports during periods of severe sparking showed that sparking always was between the discharge electrodes and plates rather than between the electrodes and bags. In spite of a total of 150,000 sparks during the 6 weeks and some arcing when water leaked into the compartment, sparks were never observed going to the bags. In addition, after pulling bags and inspecting, there was no evidence of sparking damage.

Bag samples were analyzed using a microscope to determine if the high A/C ratio caused dust penetration. Under magnification of 10–50x, the media surface was clear of particulate matter after brushing, which indicates no dust penetration into the membrane.

The air permeability analysis of the AHPC filter bag media was performed in the lab using a Frazierometer. This device measures the amount of air that flows through a flat sample of media 3.5 in. in diameter and correlates it to a Frazier number. The Frazier number describes the volume of air (ft^3/min) passing through 1 ft^2 of media at a differential pressure of 0.5 in. W.C. A Frazier number of 1.0 indicated 1 ft^3/min/ft^2 at 0.5 in. W.C. Canceling units of ft^2, the Frazier number units are expressed as ft/min at 0.5 in. W.C.

Samples of the three AHPC filter bags were cut from the top, middle, and bottom bag locations. The average Frazier numbers for the three bags were 1.9, 1.8, and 2.4 ft/min at 0.5 in. W.C. Next, the samples were carefully brushed to remove the primary dust layer from the membrane surface. The samples were retested in the exact locations to measure the permeability change after brushing. The average bag permeabilities were 3.0, 3.0, and 4.6 ft/min at 0.5 in. W.C. These media permeability values are typical of filter bags from coal-fired boiler applications. As a baseline, the new media Frazier number is generally within the range of 3.5–6.0 ft/min at 0.5 in. W.C.

SUMMARY

After 6 weeks of operation, the bags seasoned to an on-line cleaned condition filter drag of 0.5 in. W.C./ft/min, which is considered typical for a coal-fired boiler application, and there was no evidence of sparking to or across the media. The AHPC has met Phase II experimental objectives of operation, including A/C ratio of 12 ft/min, dissipation of charge and spark potential, particulate release upon pulse-jet cleaning, low-particulate matter emissions, and recoverability from AHPC system upsets.

REFERENCES

1. Oglesby, S.; Nichols, G.B. , Electrostatic Precipitation, Marcel Dekker, Inc.: New York 1978.

2. Dennis, R. et al., Filtration Model for Coal Fly Ash with Glass Fabrics, EPA-600/7-77-084 Aug 1977.

3. Leith, D.; Rudnick, S.N.; First, M.W. High-Velocity, High-Efficiency Aerosol Filtration, EPA-600/2-76-020 Jan 1976.

4. Miller, S.J., Schelkoph, G.L.; Dunham, G.E.; Krigmont, H.V.; Walker, K.E. Advanced Hybrid Particulate Collector, A New Concept for Fine Particle Control. Partec 98, International Congress for Particle Technology, 4th European Symposium Separation of Particles from Gases, Nürnberg, Germany, March 10–12, 1998.

5. Miller, S.J. Advanced Hybrid Particulate Collector, A New Concept for Air Toxics and Fine Particle Control. Presented at the Advanced Coal-Based Power and Environment Systems '98 Conference, Pittsburgh, PA, July 21–23, 1998.

TABLE 1

AHPC Specifications

Flow Rate	8646 acfm at 12 ft/min 11,520 acfm at 16 ft/min
Bags	32 (4 rows × 8 bags/row) 5.75 in. d. × 15 ft long
Bag Type	GORE-TEX® all ePTFE No-Stat®
Collection Plates	18 gauge, 29-in. spacing 14 ft 4 in. × 7 ft 3 in.
Discharge Electrodes	Rigid mast type with directional spikes toward plates
Discharge Electrode Spikes to Plate Distance	5 in.
Discharge Electrode Spike to Bag Distance	6.5 in.
Rappers	Pneumatic vibrator type for both plates and discharge electrodes
HV Power	ABB switched integrated rectifier (SIR)

TABLE 2

AHPC Dust Loadings Taken 8/18/99

Inlet		Sample
Grains/scf	% H_2O	Time
1.17	12.84	25 min
1.36	12.84	15 min

Outlet		Sample	Removal
Grains/scf	% H_2O	Time	Efficiency %
0.0000913	12.2	4 hr	99.993
0.0000398	11.8	17 hr	99.997

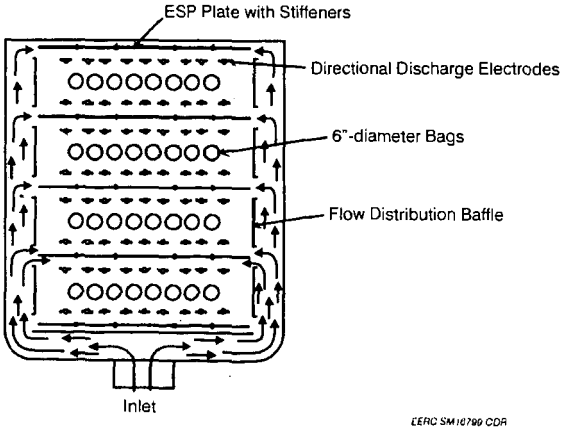

Figure 1. Top view of the 9000-acfm AHPC.

FORMATION OF ULTRA-FINE PARTICULATE MATTER FROM PULVERIZED COAL COMBUSTION

C.L. Senior and T. Panagiotou
Physical Sciences Inc.
Andover, MA 01810

Adel F. Sarofim
University of Utah
Salt Lake City, UT

Joseph J. Helble
University of Connecticut
Storrs, CT

KEYWORDS: PM2.5, coal-fired, power plants, fine particulate matter

INTRODUCTION

Although attention is focused currently on the emission of particles less than 2.5 microns (PM2.5) from stationary combustion systems, ultrafine or submicron particulate matter may prove to be an important constituent of PM2.5. Field observations[1-3] and theoretical considerations[4] lead us to conclude that vaporization and condensation of ash occurs in pulverized coal-fired power plants. Furthermore, many toxic trace elements are enriched in the vaporization mode of the fly ash[5] because many of the inorganic elements in coal are volatile at flame temperatures.[6,7] In the flame zone, the inorganic vapors homogeneously nucleate to form an ultrafine aerosol with a primary particle size of 0.01 to 0.03 μm.[8] Post-flame, the combustion gases cool rapidly to near room temperature in a time period of 2 to 5 s. The mean particle size of this condensation aerosol grows by coagulation. Calculations for a typical vapor loading show that the peak of the mass distribution grows to 0.03 to 0.07 μm in the range of 1 to 10 s.[6] These ultrafine ash particles are not collected as efficiently by electrostatic precipitators as are the larger ash particles.[9] Thus, toxic metals in the vaporization mode can be preferentially emitted to the atmosphere.

Measurements of submicron aerosol from full-scale coal-fired power plants show a distinct peak in the mass distribution falling in the range of 0.07 to 0.15 μm.[1-3,9] These measurements are made at the ESP inlet, not in the flame zone. In one study,[3] two submicron modes were observed with peak diameters at 0.07 microns and 0.4 μm. Scanning electron micrographs of the two submicrometer modes showed that the 0.4 μm particles were solid spheres, while the particles below 0.1 μm were agglomerates of ultrafine primary particles. In full-scale combustion systems, therefore, ash collected with diameters less than 0.1 to 0.2 μm could be attributed to vaporization.

The ultrafine mode can be ascribed to a vaporization-condensation mechanism.[4] Taking into account all the observations mentioned above, the ultrafine mode has a peak (mass distribution) of 0.07 to 0.15 μm. The variation in the diameter is mostly due to the combustion conditions; coal type is a second order effect. This can be seen in the data of McElroy et al.[2] Six power plants of different designs were sampled. All but one were burning western sub-bituminous coals. Data are given on the fraction of the ash found in the submicron aerosol as a function of NO content in the exhaust gas (Figure 1). Since NO is related to the peak combustion temperature, Figure 1 shows that the combustion conditions have a strong effect on the amount of mass in the ultrafine mode. The type of coal and furnace design do not seem to have a strong influence on the amount of ash in the ultrafine mode. Although, it should be noted that while this data set represents most types of boilers (except cyclone-fired), five out of six of the coals are western sub-bituminous coals.

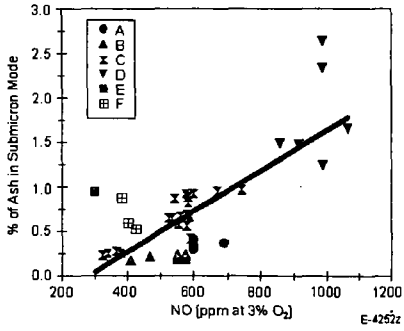

Figure 1. Mass fraction of ash in submicron mode as a function of NO for six different boilers.[2] Line is best fit ($r^2 = 0.57$).

The composition of the submicron mode from coal combustion varies with coal type. The most complete dataset is found in Quann and Sarofim.[10] This work was both experimental and theoretical. The effects of coal rank, particle size, particle temperature and oxygen concentration were examined.

Also, a theoretical analysis on vaporization from included, excluded and atomically dispersed minerals was accomplished. This analysis indicates that the element vaporization depends on one or more of the following parameters: bulk oxygen concentration, coal rank, coal type, particle size and composition of inherent ash. Results of this effort for Si, Ca and Mg were in very good agreement with the experiments.

MODEL FORMULATION

In the present work, we used the theoretical framework of Quann and Sarofim[10] to calculate the fraction of individual metal oxides (f_v) which vaporize during combustion of the char particle burning for time t_B. The total amount of metal oxides vaporized was then calculated by summing over all the major oxides. For this work, instead of calculating f_v/t_B from first principles, we used existing experimental results as reference, as described in Reference 10. The reference data were values for the fractional vaporization of a metal normalized to the char burnout time, $(f_v/t_B)_r$, the equilibrium partial pressure of the metal, p_{ir}, the concentration of the element of interest in the coal particle, C_{or}, and the coal particle radius (or diameter), r_{or} (d_{or}) for one bituminous and one low rank coal. The reference combustion conditions were a gas temperature of 1750 K and a bulk oxygen partial pressure of 0.2. The particle temperature under such combustion conditions was measured to be 2100 K.[10] The following equations that use reference data were derived from Reference 10. For an element *i* found in mineral inclusions in the char particles:

$$f_v/t_B = (f_v/t_B)_r (p_i/p_{ir})(r_{or}/r_o)(C_{or}/C_o) \quad (1)$$

For an element *i* found primarily organically-bound to the char:

$$f_v/t_B = (f_v/t_B)_r (p_i/p_{ir})(r_{or}/r_o)^2 (C_{or}/C_o) \quad (2)$$

For an element *i* found in excluded mineral particles, not contained in char:

$$f_v/t_B = (f_v/t_B)_r (r_{or}/r_o)^2 (C_{or}/C_o) \quad (3)$$

The burnout time was computed assuming diffusion-limited combution where the burnout time is proportional to the particle radius and the bulk oxygen concentration, p_{O2}:

$$t_B \propto r_o^2 / \ln(1+p_{O_2}) \quad (4)$$

The metal gaseous mole fractions, p_i and p_{ir}, are calculated by assuming that the metal oxides undergo reduction during evaporation, for example:

$$SiO_2 + CO <=> SiO + CO_2 \quad (5)$$

And the partial pressure of SiO is equal to:

$$p_{SiO}=(a_{SiO_2} K_{eq} p_{CO})^{1/2} \quad (6)$$

where a_{SiO2} is the activity coefficient and K_{eq} is the equilibrium constant. The activity coefficient is assumed to be independent of coal type and combustion conditions, so it cancels out in Eqs. (1) through (3). The equilibrium constants used were curvefits from data over a temperature range of 1500 to 2500 K as shown in Table 1.

The simple equilibria between CO and CO_2 can be used for each metal species of interest, assuming that oxygen diffusing to the char particle surface is completely consumed and that CO is

Table 1. Vaporization Equilibrium Equations and Equilibrium Coefficients - Equilibrium Constants at Temperature Char Temperature T are Calculated from $\ln(K)=A+B10^4/T$

Vaporization Equation	A	B
$Na_2O+CO=2Na+CO_2$	17.8966	-2.8487
$FeO+CO=Fe+CO_2$	11.4942	-4.2064
$SiO_2+CO=SiO+CO_2$	18.8256	-5.9700
$Al_2O_3+2CO=Al_2O+CO_2$	24.0505	-11.3361
$MgO+CO=Mg+CO_2$	14.4976	-5.4094
$CaO+CO=Ca+CO_2$	13.2182	-6.1507

the only product of combustion. In this case, the bulk oxygen concentration, p_{O2b}, will determine the concentration of CO at the surface:

$$P_{CO_s} = 2\, p_{O2b}/(1 + p_{O2b}) \tag{7}$$

The fraction of potassium vaporized was calculated from a separate equation, based on previous work which showed a good correlations between the fraction of potassium and sodium vaporized during coal combustion.[12]

$$f_{v\text{-}K} = 0.007706 + 0.6165746\, f_{v\text{-}Na} \tag{8}$$

RESULTS

For validation purposes, we used our model to predict metal vaporization from a variety of coals burning at different conditions. Subsequently, we compared our predictions with experimental data. The purpose of this effort was to assess the accuracy of our model with respect to parameters that affect vaporization and then improve the accuracy by making proper corrections. The following parameters that affect the vaporization were examined: (a) the coal type, (b) the coal rank, (c) the coal particle diameter , (d) the oxygen concentration and (e) the element concentration in the coal. A complete set of vaporization data that involved a variety of coals, particle sizes and combustion conditions was given in Reference 10. In those experiments, vaporization from excluded minerals was negligible. Therefore, in our calculations we only accounted for vaporization from included and organically bound minerals.

Initially we calculated the fraction of Si, Na, K, Ca, Fe, Al and Mg that vaporized as oxides, namely: SiO_2, Na_2O, K_2O, CaO, FeO, Al_2O_3 and MgO . Subsequently, the amounts of the individual amounts of vaporized oxides were estimated. Finally, the amounts of oxides vaporized were summed to get a calculated value of the total ash vaporized. As reference values for Eqs. (1) and (2), the following experimental data we used: (a) for vaporization of Na, Si, Fe and Al from bituminous coals, we used data for Illinois 6 from Quann,[10] and (b) for vaporization of Na, Si, Fe, Al, Ca and Mg from sub-bituminous coals and lignites, we used data for Montana Savage lignite from Quann.[10]

Vaporization of major elements was predicted for Illinois 6 considering different coal particle sizes and bulk oxygen contents. Figure 2 shows the effect of oxygen concentration on vaporization from coal particles with diameters of 50 μm and 120 μm with a gas temperature of 1750 K. The model does a good job of predicting the effect of oxygen content on total vaporization. However, the effect of coal particle diameter is not modeled as well. Vaporization for large coal particles is over-predicted by two to three times.

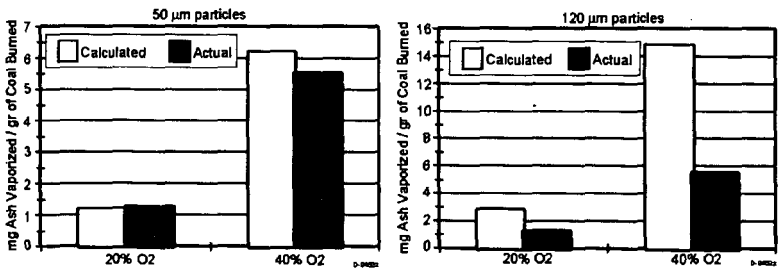

Figure 2. Effect of oxygen concentration on ash vaporization from Illinois 6 coal particles burning at a gas temperature of 1750 K for two different coal particle diameters: (a) 50 μm and (b) 120 μm.

Similar results were obtained for other bituminous coals. Figure 3 compares the amount of vaporization from 50 μm coal particles burning at a gas temperature of 1750 K for the Illinois 6 coal with two other bituminous coals. In Figure 4, the predicted and measured compositions of one of the bituminous coals are shown. The calculation tends to over-predict the amount of iron in the submicron ash for bituminous coals.

Vaporization of major elements was predicted for a Montana lignite considering different coal particle sizes and bulk oxygen contents. Figure 5 shows the effect of oxygen concentration on vaporization from low rank coal particles with diameters of 60 μm and 120 μm with a gas temperature of 1750 K. The model does a good job of predicting the effect of oxygen content and coal particle size on total vaporization.

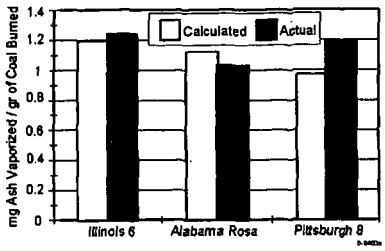

Figure 3. Predicted and measured ash vaporization from bituminous coals: 50 μm diameter particles burning in 20% oxygen with a gas temperature of 1750 K.

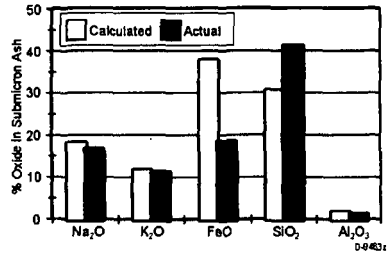

Figure 4. Predicted and measured submicron ash composition from combustion of Pittsburgh 8 coal: 50 μm diameter particles burning in 20% oxygen with a gas temperature of 1750 K.

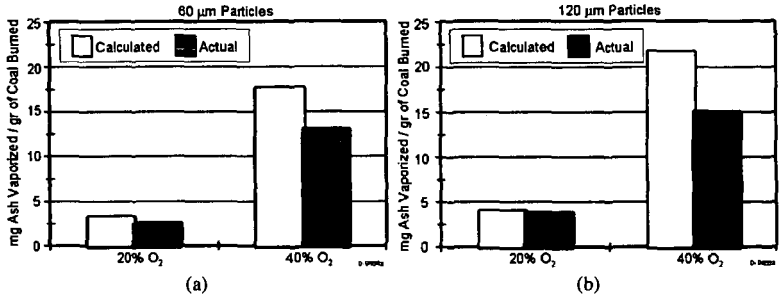

Figure 5. Effect of oxygen concentration on ash vaporization from Montana Savage lignite particles burning at a gas temperature of 1750 K for two different coal particle diameters: (a) 60 μm and (b) 120 μm.

Similar results were obtained for other low rank coals. Figure 6 compares the amount of vaporization from 60 μm coal particles burning at a gas temperature of 1750 K for the Montana Savage lignite (MO SVG L) coal with three other coals: Montana Rosebud sub-bituminous (MO RSB S), North Dakota Lignite (ND L), and Montana Powder River Basin sub-bituminous (MO PRB S).

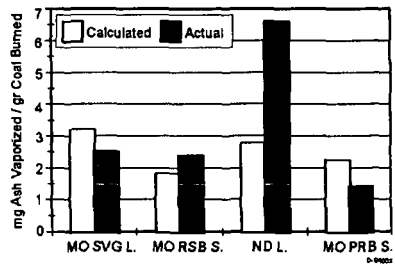

Figure 6. Predicted and measured ash vaporization from low rank coals: 60 μm diameter particles burning in 20% oxygen with a gas temperature of 1750 K. With the exception of the North Dakota lignite, the model accurately predicts the vaporization of major elements.

SUMMARY

This work aimed to develop a model that predicts the vaporization of metals during coal combustion. The model is based on other existing models, experimental data and correlations of data. The main factors that affect the metal vaporization are: the coal rank, the coal type, the coal particle size, the oxygen content (and therefore the particle temperature) and the metal concentration in the coal. Our model predicts fairly accurately the amounts of ash that vaporizes and the submicron ash composition of bituminous coals based on a fixed reference condition. The effect of oxygen concentration and the metal composition of the coal on the ash vaporization are predicted well, but the effect of the coal particle diameter is not predicted accurately. Our model predicts fairly accurately the amounts of ash that vaporizes and the submicron ash composition from a variety of low rank coals based on a fixed reference condition. The model predicts the effect of coal particle size on the ash vaporization better than it does the effect of oxygen concentration, unlike the case of the bituminous coals. The modeling efforts should concentrate on the following areas: (a) the effects of coal particle size and oxygen concentration on the element evaporation and (b) the accuracy of iron and alkali vaporization.

REFERENCES

1. Schmidt, E.W., Gieseke, J.A., and Allen, J.M. "Size Distribution of Fine Particulate Emissions from a Coal-Fired Power Plant," *Atm.Env.*, **1976**, *10*, 1065-1069.
2. McElroy, M.W., Carr, R.C., Ensor, D.S, and Markowski, G.R. "Size Distribution of Fine Particles from Coal Combustion," *Science*, **1982**, *215*, 13-19.
3. Joutsenaari, J., Kauppinen, E.I., Jokiniemi, J.K., and Helble, J.J. "Studies on Ash Vaporization in Power Plant Scale Coal Combustion," in *The Impact of Ash Deposition on Coal Fired Plant*, J. Williamson and F.Wigley, editors, Washington, D.C.: Taylor & Francis, 1994, pp. 613-624.
4. Flagan, R.C and Friedlander, S.K., "Particle Formation in Pulverized Coal Combustion: A Review," in *Recent Developments in Aerosol Science*, D.T. Shaw, Ed., Wiley, New York, 25-59 (1978).
5. Davison, R.L., Nautusch, D.F.S., and Wallace, J.R. "Trace Elements in Fly Ash Dependence of Concentration of Particle Size," *Environ.Sci.Technol.*, **1974**, *8*, 1107-1113.
6. Linak, W.P. and Wendt, J.O.L. "Trace metal transformation mechanisms during coal combustion," *Fuel Process.Tech.*, **1994**, *39*, 173-198.
7. Fransden, F., Dam-Johansen, K. and Rasmussen, P.R. "Trace Elements from Combustion and Gasification of Coal–An Equilibrium Approach," *Prog.Energy.Comb.Sci.*, **1994**, *20*, 115-138.
8. Helble, J.J. and Sarofim, A.F. "Factors Determining the Primary Particle Size of Flame Generated Inorganic Aerosols," *J. Colloid Interface Sci.*, **1989**, *128*, 348-362.
9. Ylätalo, S.I. and Hautanen, J., "Electrostatic Precipitator Penetration Function for Pulverized Coal Combustion," *Aerosol Sci.Technol.*, **1998**, *29*, 17-30.
10. Quann, R.J., Neville, M., Janghorbani, M., Mims, C.A., and Sarofim, A.F. "Mineral Matter and Trace-Element Vaporization in Laboratory-Pulverized Coal Combustion System," *Environ.Sci.Technol.*, **1982**, *16*, 776-781.
11. Senior, C.L. et al., "Toxic Substances from Coal Combustion – A Comprehensive Assessment," Phase I Final Report, DOE Contract DE-AC22-95PC95101, September 1997.
12. Bool, II, L.E., Helble, J.J. Shah, N., Shah, A., Huffman, G.P., Huggings, F.E., Rao, K.R.P.M., Sarofim, A.F., Zeng, T. , Reschke, R., Gallien, D. and Peterson, T.W. "Fundamental Study of Ash Formation and Deposition: Effect of Reducing Stochiometry," Final Report prepared for Department of Energy, PETC, under Contract No. DE-AC22-93PC92190, PSIT-1178/TR-1407, September 1995.

The Effect of Blending Coals on Electrostatic Precipitator Performance

Belinda Wheland, Glenn Devire, **John H. Pohl**,
Department of Chemical Engineering,
University of Queensland, Brisbane, Queensland, 4072, Australia

Robert A. Creelman
R.A Creelman and Associates
Epping, New South Wales, 2121, Australia

Key Words: electrostatic precipitation, particulate emission, fly ash, coal, boilers

ABSTRACT

Tarong Power Station, in southern Queensland, Australia, operates 4 X 350 Mwe coal-fired boilers. The boilers fire the local, Meandu Coal from the isolated Tarong Basin. This coal contains 0.3 percent sulfur and 27 percent ash. This ash is 71 percent SiO_2, 27.5 percent Al_2O_3, and 1.9 percent TiO_2, with small amounts of other components. This coal has poor precipitation performance. With water injection, these plants emit 470 mg/Nm^3 of particulate matter. Recent power plant trials blending Meandu with Jeebropilly coal from the Morton Basin (near Ipswich) and Wilke Creek Coal from the Surat Basin (near Dalby) with Meandu Coal have reduced the emissions to near 100 mg/Nm^3.

The objective of this study was to identify the causes of the improved precipitator performance when Meandu Coal was blended with other coals and to determine the properties of other coals that would improve the precipitator performance. We gathered emission data from the power plant trials, measured particle size, and analyzed the fly ash for chemical composition, and electrical resistivity. We calculated drift velocities that confirm that Meandu fly ash is difficult, but Jeebropilly and Wilke Creek are easier to collect. We attributed the small difference between calculated and measured efficiency to the effect of ash resistivity. For the conditions studied, the difference in efficiencies did not primarily depend on particle size or sulfur concentration, but were related to the concentrations of alkali and alkaline earth metal in the fly ash.

INTRODUCTION

Many Australian Coal are considered difficult to precipitate. This is attributed to the low sulfur concentration of the coals and high quartz content of coal ash. This has been a consideration in purchasing Australian Export Coals for some time. Recently, Australia has begun to impose particulate emission standards on coal-fired power plants. Most of the power plants in Australia use Electrostatic Precipitators (ESP) to collect fly ash. Many Australian Coals are low in sulfur and the ashes are high in quartz. These fly ashes are difficult to collect in ESP's. The Meandu Coal, from the isolated Tarong basis, burned at Tarong Power Station has a fly ash that is particularly difficult to collect using an ESP. Table 1 shows that the Meandu Coal has 0.3 percent sulfur and 27 percent ash. The ash from Meandu Coal has 71 percent SiO_2, 27.5 percent Al_2O_3, 1.9 percent TiO_2, and small amounts of other constituents[1]. Table 2 shows that the Meandu Coal, using water injection, has an emission of 470 mg/Nm^3. However, blending the Meandu coal with Jebroopilly Coal, from the Morton basin near Ipswich or Wilke Creek Coal, from the Saurat Basin near Dalby[1], improved the emissions to around 100 mg/Nm^3. The purpose of this paper is to determine the cause of the improved collection efficiency when Meandu Coal is blended with Wilke Creek or Jebroopilly Coal.

ESP PERFORMANCE

The collection efficiency of an ESP is controlled by the Deutsch Equation[2-4]:

$$\eta=100 \times [1-\exp(-w \times SCA)]$$

where η= the collect in percent
w = the drift velocity in m/s
SCA = the specific collection area in m^2/m^3-s

The drift velocity can be estimated by[3]:

$$W = k \times \varepsilon \times \varepsilon_0 \times E^2 \times d_{m50} / (\varepsilon + 2) \times \mu$$

where: $k = 1/7$ = ratio of effective drift velocity to theoretical drift velocity
ε = dielectric constant of the dust
$\varepsilon_0 = 8.85 \times 10^{-12}$ F/m = permittivity of free space
E = electric field strength v/m
d_{m50} = mass mean diameter of particles m
μ = gas viscosity Pa.s

Table 1. Coal Properties[1]

% AD	MEANDU	WILKE CREEK	JEBROOPILLY
H_2O	2.9	8.0	4.1
ASH	26.9	13.0	14.3
VOLATILES	27.5		39,8
% DAF			
C	79.5		81.1
H	5.43		6.38
N	1.45		1.61
S	0.37	0.5	0.70
O(DIFF)	13.3		10.2
% ASH			
SiO_2	71.0		61.9
Al_2O_3	27.5		32.7
Fe_2O_3	0.74		1.58
CaO	0.26	1.75	0.74
MgO	0.11	1.40	0.74
Na_2O	0.03	0.80	1.10
K_2O	0.30	0.40	0.66
TiO_2	1.86		2.13
Mn_3O_4	0.01		0.01
SO_3	0.04	0.60	0.22
P_2O_5	0.02		0.04
BaO	0.02		0.07
SrO	0.02		0.06
ZnO	0.02		0.01

The ability to collect fly ash particles with an ESP depends on[5]: fundamental, mechanical, and operational limitations. In this paper, we investigate the fundamental problems associated with the characteristics of the fly ash and gas. These problems include:

- Particle
  - Resistivity
  - Size distribution
  - Strucrure
  - Density
  - Composition
  - Concentration
  - Agglomeration
- Gas
  - Temperature
  - Moisture
  - Flow

The ESP's at Tarong operate at 140 C, use water injection, and seem to have adequate flow patterns. We therefore concentrated on the properties of the particles that effect ESP collection efficiency.

Particle size did not seem to have a major effect on the collection efficiency for the coals studied. However, the nature of the fly ash particles did. We found resistivity to be the most important fly ash property.

The ESP's at Tarong operate at 20 kv over a 150 mm^3 spacing. This is a low voltage. It is restricted by the breakdown and charging of the gas in the high gradient regions between particles. The potential could be increased if the particle resistivity was reduced.

EXPERIMENTAL

Tarong Power Station provided operating data and samples of the coal and resulting fly ash. The samples were analyzed for particle size distribution, chemical composition, and resistivity. Australian Industrial Coal Research Laboratory (ACIRL) performed the analyses[6].

RESULTS

Table 2. shows the plant measurements for the Trials of Meandu Coal blended with Wilke Creek.

Table 2. Operating Performance of Meandu and Wilke Creek Coals[3,7,8,9]

COAL	100 % MEANDU	50 % WILKE CK	100% WILKE CK
COAL T/H	170	138	138
% ASH	29.7	21.3	12.8
GAS DEN @140	0.88	0.88	0.88
FLUE GAS KG/S	626.2	627.6	689.1
IN DUST g/Nm^3	15.9	9.2	5.0
OUT DUST g/Nm^3	470	107	67
ESP EFF	97.0	98.8	98.8

Table 3. shows estimated efficiencies based on the Deutsch Equation. Baker, et al[6], measured the dieletric constant for Meandu Coal as 1.79 and for Blackwater Coal (similar to Jeebropilly and Wilke Creek Coal) as 7.33. Here, we assume the dieletric constants for Jeebropilly and Wilke Creek Coals are about 10.

Table 3. Calculated Drift Velocities and ESP Efficiencies

COAL	100 % MEANDU	50 % JEEBROPILL	100 % JEEBROPILL	10 % WILKE CREEK
W cm/s	1.48	1.56	1.62	2.02
CAL EFF	97.87	98.27	98.50	99.47

Figure 1. shows that increasing alkali and alkaline earth metal concentration reduces the Meandu and Jeebropilly fly ash resistivity.

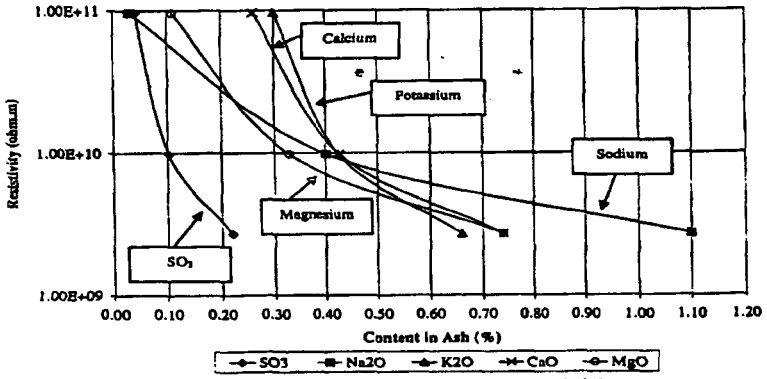

Figure 4.8: Influence of ash properties on resistivity

DISCUSSION

We find that the alkali and alkaline earth metal concentrations are the most important factors reducing the resistivity of the fly ash. This is consistent with earlier findings. Bush and Snyder[10] found that sulfur, alkali metals, and water have the largest influence on fly ash resistivity. Harker and Pimparkar[11] reported that sulfur had limited effect on fly ash resistivity. Bush and Synder[10], Bickelhaupt[12], Tidy[13], and White[14] now believe that the concentration of alkaline metals on the surface of fly ash particles are the most important factor in reducing resistivity.

Bush and Sydner[10] suggest that calcium and magnesium also reduce resistivity. Bickelhaupt[12] argues that potassium and lithium are key components in reducing ash resistivity. Tidy[13] showed

that calcium, magnesium, lithium, and potassium were present on the surface of fly ash particles, but were less important in reducing resistivity than sodium. Bickelhaupt[12] thinks the reduced resistivity may be a combination of the above metals.

We find that all the alkali and alkaline earth metal reduce fly ash resistivity. The metals with the smallest ionic radii reduce fly ash resistivity the most for the coals studied. However, lithium concentration was not measured in the current study.

RECOMMENDATIONS

We will measure the lithium concentrations on the fly ash samples. In addition, we will do pilot scale combustion and ESP trials to determine the optimum amount of coal and type of coals to blend and to investigate the effect of injecting solutions of alkali and alkaline earth salts into the duct.

ACKNOWLEGMENTS

The authors would like to acknowledge the help Tarong Power Station gave to this project. They would also like to acknowledge the work that ACIRL, Ipswich, did.

REFERENCES

1. Queensland Coals: Chemical and Physical Properties, Queensland Coal Board, Brisbane, Queensland AUSTRALIA.
2. Potter, E. C., Electrostatic Precipitator Technology: A Different Viewpoint, J. Air Pollution Control Association, 28 (1), pp40-46, January 1978.
3. Johnson, M., The Effect of Humidity on the Performance of Electrostatic Precipitators at Tarong Power Station, BE Thesis, Queensland University of Technology, Brisbane, Queensland AUSTRALIA 1996.
4. Bohm, J., Electrostatic Precipitators, Elsevier Scientific, Amsterdam, Netherlands, 1982.
5. White, H.J. Industrial Electrostatic Precipitation, Addison - Wesley, MA, USA, 1963.
6. Baker, J.W., P.D. Smith, and K.M. Sullivan, Electrostatic Precipitation Research Part A – Electrical Properties, Australian Coal Research Laboratories Ltd., Department of Resources, Canberra, ACT AUSTRALIA.
7. ERM Consultants Pty Ltd., AQC Surat Coal at Tarong, 1996.
8. Harridge, D. Flue Gas Dust Burden Test Results - 10% Wilke Creek Blend, Tarong in- house report, 1998.
9. Bush, P. V. and T.R. Synder, Implication of Particulate Properties on Electrostatic Precipitator Performance and Fabric Filter Performance, Powder Technology, 72, pp.207-213, 1992.
10. Harker, J. R. and P. M. Pimparkar, The Effect of Additives on Electrostatic Precipitation of Fly Ash, J. Institute of Energy, pp.134-142, September 1999.
11. Bickelhaupt, R. E. , Surface Resistivity and chemical Composition of Fly Ash, J. Air Pollution Control Association, 25 (2), pp. 148-152, February 1975.
12. Tidy, D., Measurement of Resistivity Relevant to the Electrostatic Precipitation of Pulverised Fly Ash, J. Institute of Energy, pp.49-58, March 1986.
13. White, H. J., Resistivity Problems in Electrostatic Precipitation, J. Air Pollution Control Association, 24(4), pp. 314-338, April 1974.